Brain-wide arousal signals are segregated from movement planning in the superior colliculus

Richard Johnston[1, 2, 3] and Matthew A. Smith[1, 2, 3]

[1]Department of Biomedical Engineering, Carnegie Mellon University, Pittsburgh, USA; [2]Neuroscience Institute, Carnegie Mellon University, Pittsburgh, USA; [3]Center for the Neural Basis of Cognition, Carnegie Mellon University, Pittsburgh, USA.

Corresponding author:
Matthew A. Smith, PhD
Carnegie Mellon University
4400 Fifth Ave.
Pittsburgh
PA, 15213
Email: mattsmith@cmu.edu

Abstract

The superior colliculus (SC) is traditionally considered a brain region that functions as an interface between processing visual inputs and generating eye movement outputs. Although its role as a primary reflex center is thought to be conserved across vertebrate species, evidence suggests that the SC has evolved to support higher-order cognitive functions including spatial attention. When it comes to oculomotor areas such as the SC, it is critical that high precision fixation and eye movements are maintained even in the presence of signals related to ongoing changes in cognition and brain state, both of which have the potential to interfere with eye position encoding and movement generation. In this study, we recorded spiking responses of neuronal populations in the SC while monkeys performed a memory-guided saccade task and found that the activity of some of the neurons fluctuated over tens of minutes. By leveraging the statistical power afforded by high-dimensional neuronal recordings, we were able to identify a low-dimensional pattern of activity that was correlated with the subjects' arousal levels. Importantly, we found that the spiking responses of deep-layer SC neurons were less correlated with this brain-wide arousal signal, and that neural activity associated with changes in pupil size and saccade tuning did not overlap in population activity space with movement initiation signals. Taken together, these findings provide a framework for understanding how signals related to cognition and arousal can be embedded in the population activity of oculomotor structures without compromising the fidelity of the motor output.

Introduction

For humans and animals to effectively interact with a fast-changing environment, they must be adept at performing a range of visually-guided motor actions. Basic everyday tasks that are critical for our survival (e.g. making an eye movement to a car that is about to cross our path) require visual information to be rapidly encoded and transformed into a motor action. In non-mammals such as birds, reptiles and fish, visually-guided motor actions (e.g. prey capture) are generated by circuits in the optic tectum (Wylie et al., 2009; Kardamakis et al., 2015; Suzuki et al., 2019; Allen et al., 2021; Isa et al., 2021) whereas in mammals such as rodents, cats and monkeys they are supported by activity in a homologous structure called the superior colliculus (SC) (Wurtz and Albano, 1980; Sparks and Mays, 1990; Gandhi and Katnani, 2011; Cang et al., 2018; Wheatcroft et al., 2022; Hafed et al., 2023).

The SC resides in the roof of the brainstem and receives input from retinal ganglion cells (Perry and Cowey, 1984; Qu et al., 2006), the primary visual cortex, and extrastriate areas such as V4 and the middle temporal area (Cerkevich et al., 2014). In addition to these visual inputs, research has shown that it also receives projections from cortical regions that have been implicated in eye movement control including the supplementary eye field (Huerta and Kaas, 1990; Parthasarathy et al., 1992) and the frontal eye field (Komatsu and Suzuki, 1985; Stanton et al., 1988; Parthasarathy et al., 1992). The role of these projections in the visuomotor transformation depends on the functional layer of the SC in which they terminate. Decades of research has shown that the SC comprises three main layers each of which contains cells with distinct neurophysiological response properties (May, 2006; Krauzlis et al., 2013; Basso and May, 2017). For example, neurons in the superficial layers, which are thought to represent the earliest stage of the visuomotor transformation, only respond to visual stimuli presented within their receptive field

70 (RF) (Goldberg and Wurtz, 1972). In contrast, neurons in the intermediate layers elicit a response
71 during both the presentation of visual stimuli and when saccades are made into their RF. Finally,
72 neurons in the deep layers primarily respond in and around the time of a saccade. As is the case
73 for neurons in the intermediate layers, they form a topographically organized map of visual space
74 (Robinson, 1972; Katnani and Gandhi, 2011; White et al., 2017) and encode saccades across a
75 range of directions and amplitudes (Gandhi and Katnani, 2011). Deep-layer SC neurons project to
76 downstream nuclei innervating the extraocular muscles (e.g. the central mesencephalic reticular
77 formation) (Sparks, 1986; Sparks and Hartwich-Young, 1989; Bohlen et al., 2017) but thresholds
78 for evoking saccades using electrical microstimulation are often lowest in the intermediate layers
79 (Mohler and Wurtz, 1976) suggesting that the intermediate and deep layers of the SC function
80 together to control saccadic eye movements (Wurtz and Albano, 1980).

81 Although the SC is best known for its role in visually-guided motor actions, our
82 understanding of its function has evolved considerably and recent work has demonstrated its role
83 in processes linked to higher order cognition (Knudsen, 2011; Krauzlis et al., 2013; Clark et al.,
84 2015; Basso et al., 2021). For example, behavioral performance on covert attention tasks (in which
85 subjects are cued to attend to a stimulus presented at a specific portion of visual space) is
86 modulated when the activity of SC neurons with RFs at the cued location are perturbed using
87 reversible inactivation or microstimulation (Müller et al., 2005; Zénon and Krauzlis, 2012). In
88 addition to cognitive signals, the SC is interconnected with brain regions that control arousal
89 levels, e.g. the locus coeruleus (LC) (Edwards et al., 1979; Aston-Jones and Cohen, 2005; Sara
90 and Bouret, 2012; Li et al., 2018; van den Brink et al., 2019; Plummer et al., 2020; Benavidez et
91 al., 2021). Several studies using microstimulation have been able to establish a link between SC
92 activity and non-invasive markers of arousal such as pupil size (Wang et al., 2012, 2014; Joshi et

al., 2016; Wang and Munoz, 2021). Furthermore, research has shown that oculomotor behavior is impacted by changes in arousal (Di Stasi et al., 2013). For example, participants are faster at initiating visually-guided saccades to peripheral target stimuli when a startling auditory stimulus is presented prior to the onset of the target (Castellote et al., 2007). These changes, which are thought to reflect increased levels of arousal, are accompanied by increased pupil size and decreased microsaccade rate even when participants perform auditory tasks that do not necessitate saccadic eye movements (Contadini-Wright et al., 2023).

To support signals related to higher-order cognition, the SC has had to undergo a number of adaptations (Basso et al., 2021). The precise details of how conserved neuronal cell types give rise to complex processes such as spatial attention has yet to be fully elucidated. However, it must occur in a manner that does not interfere with the signals needed for volitional control of the eyes be it in the context of stable fixation or large amplitude saccades. As is the case for cortical regions that have a direct influence on motor behavior, having signals related to higher-order cognition and brain state intermingled with those used for movement encoding could be problematic as it may lead to interference with motor planning via premature or unwanted muscle contractions. In the motor cortex, research using delayed-reach tasks has shown that population responses during movement preparation are kept separate from those used during movement initiation (Kaufman et al., 2014; Elsayed et al., 2016). Furthermore, visual and motor responses in the SC occupy separate subspaces when they are recorded during the same oculomotor task and across different tasks which could facilitate the decoding of signals related to sensation, action and context by downstream regions (Jagadisan and Gandhi, 2022; Ayar et al., 2023). We hypothesized that a similar mechanism might exist in the SC to prevent arousal-related fluctuations from interfering with eye movement outputs.

In this study, we observed arousal-related fluctuations in the spiking responses of neuronal populations in the SC while monkeys performed a task that is commonly used to study visually-guided motor actions. By using dimensionality reduction on the neural population data, we were able to identify an axis in population activity space that was similar to the "slow drift axis" that has been observed in several cortical areas (Cowley et al., 2020) and is known to be associated with a constellation of arousal-related variables including pupil size and alpha power as measured using scalp electroencephalography (EEG) (Johnston et al., 2022a, 2022b). Importantly, we found evidence that this signal is isolated from SC neurons with strong saccadic responses: the activity of these cells was less correlated with the slow drift axis when it was computed using population activity in the SC and simultaneously recorded data in the prefrontal cortex (PFC). Finally, we were able to show that signals in the SC that are used to control the size of the pupil reside in an orthogonal subspace to those that are used for saccade generation. This provides a potential mechanism through which signals related to cognition and arousal can exist in the SC, and even impact processing at the early to mid-stages of the visuomotor transformation, without leading to unwanted changes in SC neurons that are most active around the time of a saccade.

Results

138 To determine how arousal-related signals related to motor-related activity in the SC, we
139 trained two monkeys to perform a memory-guided saccade task (MGS) task (Figure 1A). During
140 the task, subjects maintained fixation on a central point while a brief target stimulus was presented
141 in the periphery. The subjects had to remember the location of this stimulus during a delay period
142 and make a saccade to that location when the fixation point was extinguished. While the subjects
143 performed the task (Monkey Do = 25 sessions, Monkey Wa = 26 sessions), we recorded the spiking
144 responses of neuronal populations in: 1) the SC using a 16-channel linear microelectrode array;
145 and 2) the PFC (area 8Ar) using a 96-channel "Utah" array (Figure 1B).

146 To determine the neurophysiological response properties of individual SC neurons, we
147 took advantage of the fact that the MGS task contains distinct epochs that can dissociate visual
148 responses from those occurring during the execution of saccadic eye movements (Hikosaka and
149 Wurtz, 1983) (Figure 1A). For each neuron, peri-stimulus time histograms (PSTHs) were
150 computed relative to: 1) the onset of the target stimulus; and 2) the onset of the saccade to the
151 remembered target location (Figure 1B). We found that some of the neurons exhibited a visual
152 response shortly after the presentation of the stimulus and a saccadic response when an eye
153 movement was made to the remembered target location (Figure 1B, Example neuron 1),
154 traditionally termed visuomotor neurons, and were present mostly on the upper and middle
155 recording contacts of our linear array. Others only exhibited a saccadic response (Figure 1B,
156 Example neuron 2), traditionally termed motor neurons, and were present mostly on the lower
157 recording contacts of our linear array. Based on what is known about the response properties of
158 neurons in the SC, these findings suggest that our linear array recordings targeted neurons residing
159 at the mid to late stages of the visuomotor transformation i.e. the intermediate and deep layers of
160 the SC (Basso and May, 2017).

To quantify the observations we made about the strength of the saccadic response, we computed a motor index for each neuron (see Methods). SC neurons with a higher motor index (i.e. those with a stronger saccadic response relative to a baseline) were assumed to reside closer to the motor output stage of the visuomotor transformation than neurons with a lower motor index. Across sessions, we found that the mean motor index for all recorded SC neurons was 0.2761 (SD = 0.1924) (Figure 1 - figure supplement 1). Neurons recorded on deeper contacts tended to have a higher motor index in most sessions (see Figure 3A for an example), though our sampling was not equal across sessions and in some cases we found mostly visuomotor or mostly motor neurons across the responsive contacts on the linear array.

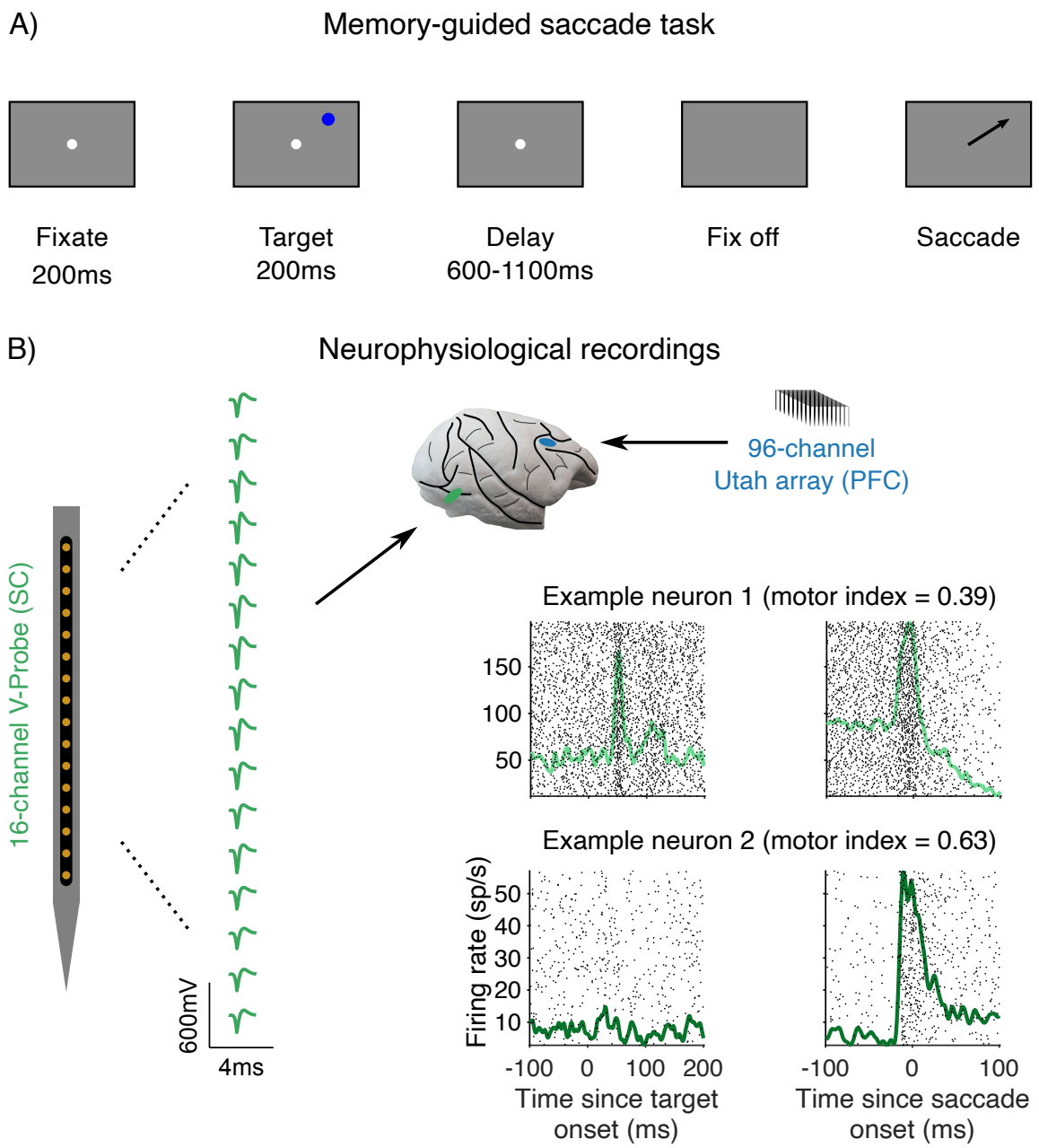

Figure 1. Experimental methods. (A) Memory-guided saccade task. After an initial fixation period, a target stimulus was presented at one of eight peripheral locations. This was followed by a delay period, the duration of which was chosen at random from a uniform distribution spanning 600-1100ms. The subjects' task was to remember the location of the target stimulus and make a saccade to it when the fixation point was extinguished. (B) Neurophysiological recordings. The spiking responses of neuronal populations in the SC were recorded for targets that were visually identified to be within the neuron's RF by applying low-amplitude microstimulation to contacts along the linear microelectrode array to evoke saccades (see Methods). The 16-channel linear microelectrode array was lowered into the brain through a recording chamber and the mean waveform for each channel during a single recording session is shown alongside a schematic of the linear array for one session. PSTHs aligned to target onset (left) and saccade onset (right) were computed to determine the response properties of individual SC neurons. Firing rates were computed in 1ms bins, averaged across trials, and smoothed using a Gaussian function for visualization purposes only (σ = 5ms).

200 Arousal-related fluctuations are present in the SC and correlated with pupil size and fluctuations
201 in PFC activity

202 We first asked if arousal-related fluctuations are present in the SC. As in previous studies
203 that recorded from neurons in the cortex (Cowley et al., 2020), we found that the mean spiking
204 responses of individual SC neurons during the delay period (chosen at random on each trial from
205 a uniform distribution spanning 600-1100ms, see Methods) fluctuated over the course of a session
206 while the monkeys performed the MGS task (Figure 2A, left). Note that this effect cannot be
207 attributed to signals related to stimulus or saccade tuning as residual spike counts were computed
208 by subtracting the mean response to each target location from trial-to-trial responses to each target
209 location. These fluctuations are also not likely to reflect instabilities in our linear array recordings,
210 as several steps were taken to remove neurons that exhibited changes in waveform shape over time
211 or large sudden changes in activity level (see Methods).

212 To identify coordinated fluctuations in activity across the population of neurons, we
213 applied PCA to residual spike counts of individual neurons during the delay period that had been
214 binned using a 15-min sliding window stepped every 3 mins. This yielded a vector of loadings
215 (Figure 2A, middle) that we termed the "slow drift axis" in line with previous studies (Cowley et
216 al., 2020). The value of each loading corresponds to the correlation coefficient between the binned
217 response of each SC neuron and the axis in population activity space that explained the most
218 variance in the data. Thus, neurons whose residual activity fluctuated more over the course of a
219 recording session had a greater portion of their variance explained by the slow drift axis (e.g.
220 Figure 2A, Channel 2). After we identified this axis from the binned data, we then projected the
221 residual responses of each SC neuron on single trials, which resulted in a single dimension along
222 which we examined fluctuations over time (Figure 2A, bottom right). When the data were pooled

223 across sessions, we found that the median proportion of variance explained by the slow drift axis
224 was 0.88 (Figure 2A, top right). By comparing the actual distribution of values to a null distribution
225 that was generated by shuffling the trial-to-trial spike counts for each neuron prior to performing
226 PCA, we were able to show that the variance explained by the slow drift axis was significantly
227 greater than what would be expected by chance ($p = 0.0385$). Note also that the dynamics of the
228 SC slow drift were highly similar when it was computed using spiking responses during the
229 baseline, visual and saccade epochs (Figure 2 - figure supplement 1). These findings suggest that
230 arousal-related fluctuations are present throughout different task epochs and are less evident in
231 deep-layer SC neurons independent of the time window in which spiking responses were
232 computed.

233 To investigate if the SC slow drift axis was related to a global signal that might be related
234 to shifts in arousal, we computed an identical axis using simultaneously recorded PFC data. If the
235 SC slow drift axis represented an arousal axis that reflected coordinated activity fluctuations
236 throughout the brain, one would expect it to be correlated with simultaneously recorded data in the
237 PFC. For each session, we computed the correlation (Pearson's product-moment correlation
238 coefficient) between projections onto the SC slow drift axis and projections onto the PFC slow
239 drift axis. As shown in Figure 2B, we found that the median variance explained across sessions,
240 as measured using the coefficient of determination (r^2), was 0.2627. To determine whether or not
241 this effect was statistically significant, we compared the actual distribution of r^2 values to a null
242 distribution that was generated by shuffling across sessions and recomputing the correlation
243 between projection values. We found that the proportion of variance explained was significantly
244 greater than what would be expected if there was no correlation between projections onto the SC
245 slow drift axis and the PFC slow drift axis ($p = 0.0190$). These findings suggest that slow

246 fluctuations in responsivity are present in populations of SC neurons, and furthermore that they
247 are coordinated across the brain. To further explore how they relate to changes in arousal or brain
248 state, we next asked if the SC slow drift axis is associated with eye metrics that are known to be
249 correlated with arousal levels.

250 Decades of research has shown that the size of the pupil can be used as a reliable marker
251 of arousal (Mathôt, 2018; Joshi and Gold, 2020). Heightened levels of arousal are accompanied
252 by concomitant increases in LC activity and pupil size (Aston-Jones and Cohen, 2005; Murphy et
253 al., 2014; Joshi et al., 2016; Reimer et al., 2016; de Gee et al., 2017; Breton-Provencher and Sur,
254 2019). Thus, we next sought to explore if projections onto the SC slow drift axis were associated
255 with pupil size. For each session, we computed the correlation (Pearson's product-moment
256 correlation coefficient) between projections onto the SC slow drift axis and mean pupil size during
257 the first 200ms of the delay period when a task-related pupil response could be observed. Across
258 sessions, we found that the median variance explained between projections onto the SC slow drift
259 axis and pupil size was 0.0597 (Figure 2C). When the actual distribution of values was compared
260 to an across-session shuffle distribution, we found that the proportion of variance explained was
261 significantly greater than what would be expected if there was no correlation between SC slow
262 drift and pupil size ($p < 0.001$). Interestingly, the median variance explained between projections
263 onto the SC slow drift axis and other eye metrics including microsaccade rate was much smaller
264 ($r^2 = 0.0026$, $p < 0.001$) (Figure 2 - figure supplement 2). Although microsaccade rate (i.e. the
265 number of small eye movements made during a period of steady fixation) has been linked to
266 arousal (Siegenthaler et al., 2014; Johnston et al., 2022a; Contadini-Wright et al., 2023),
267 microsaccade rates are task-dependent (Winterson and Collewijn, 1976; Ko et al., 2010; Bowers
268 et al., 2021) and may be driven by activity in cortical as opposed to subcortical regions (Hafed et

al., 2021). This might explain why no significant correlation was found between SC slow drift and microsaccade rate in the present study.

Taken together, these findings point to a link between the SC slow drift axis and brain-wide arousal signals. That simultaneously recorded PFC data and pupil size were correlated with projections onto the slow drift axis suggests that the signal we identified in the SC is highly similar to that which has been observed across several cortical areas (Cowley et al., 2020; Hennig et al., 2021). The fact that signals related to arousal are present in the SC is not particularly surprising given that its functional role has evolved and is now thought to include higher order cognitive processes (Knudsen, 2011; Krauzlis et al., 2013; Clark et al., 2015; Basso et al., 2021). However, it also poses a problem. Given the well-established role of deep-layers SC neurons in saccade generation (Sparks and Hartwich-Young, 1989; Gandhi and Katnani, 2011), having signals related to cognition and arousal embedded in oculomotor circuits that send gaze commands to downstream nuclei could lead to unwanted changes in eye position. One possibility is that arousal-related fluctuations are isolated from these deep-layer SC neurons that reside closer to the motor output. If this is the case, one would expect neurons with a stronger saccadic response to minimally fluctuate over time, and have a smaller portion of their variance explained by fluctuations along the slow drift axis.

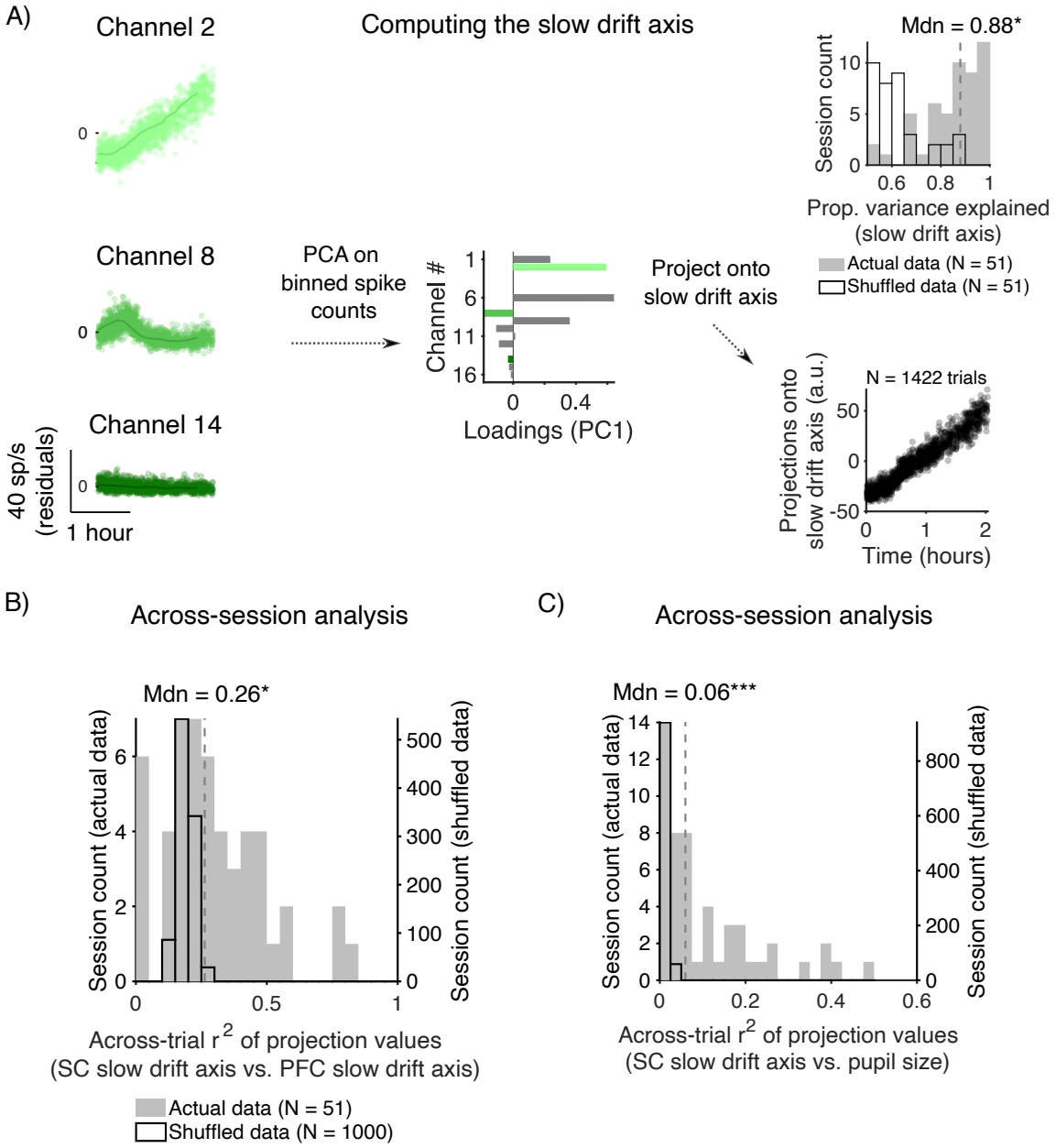

Figure 2. Arousal-related fluctuations are present in the SC and correlated with pupil size and fluctuations in PFC activity. (A) Computing the slow drift axis. Three example SC neurons from the same recording session (left). Each point represents the mean residual firing rate during the delay period. When PCA was applied to binned spike counts (solid line overlaid on each neuron's spike count residuals) it yielded a vector of loadings for the first principal component, which we will term the "slow drift axis" (middle). trial-to-trial residual SC responses during the delay period were then projected onto this vector (bottom right). The histogram in the top right shows the proportion of variance explained by the slow drift axis across sessions. The median value is indicated by the vertical dashed line overlaid on the histogram. A p-value was computed by comparing the actual distribution of values to a shuffled distribution (see Methods). (B) Histogram showing the proportion of variance explained between projections onto the SC slow drift axis and projections onto the PFC slow drift axis. Note that in this analysis, the slow drift axis was computed separately for each region using the method shown in (A). Trial-to-trial residual SC responses during the delay period and trial-to-trial residual PFC responses were then projected onto the SC slow drift axis and the PFC

slow drift axis, respectively. The median value across sessions is denoted by the vertical dashed line overlaid on the histogram. A p-value was computed by comparing the actual distribution of values to a shuffled distribution (see Methods). (C) Same as (B) but in this case the histogram shows the proportion of variance explained between projections onto the slow drift axis and pupil size. $p < 0.05$*, $p < 0.01$**, $p < 0.001$***.

Arousal-related fluctuations are isolated from SC neurons with a higher motor index

To investigate if arousal-related fluctuations are isolated from deep-layer SC neurons, we took advantage of the fact that our linear array recordings targeted neurons residing in earlier and later stages of the visuomotor transformation (Figure 1B). As described above, this was quantified by computing a motor index for each SC neuron with high values indicating that a cell elicited a strong saccadic response to the remembered target location and low values indicating that a cell elicited a weak saccadic response. Cells with a higher motor index tend to reside in the deep layers of the SC closer to the motor output (Basso and May, 2017). In several sessions, such as that shown in Figure 3A, we observed that the loadings for the slow drift axis (i.e. the correlation between the response of each neuron and the component that explained the most variance in the data) were weaker for neurons with a higher motor index. Of note in this particular session is that these neurons were recorded from channels at the bottom of the probe, which presumably targeted the deep layers of the SC.

To explore if a similar effect was found across sessions, we computed the squared component loading for all recorded SC neurons. This was done to control for the fact that the sign of the correlation between the response of each neuron and the slow drift axis is arbitrary and could be positive or negative (Jolliffe and Cadima, 2016). Next, we discretized the motor indices of all recorded SC neurons into four equally spaced bins. Permutation tests were then performed across the four bins to investigate if neurons with a stronger saccadic response explained less variance in the slow drift axis. After controlling for multiple comparisons (Bonferroni correction), we found

that the mean squared component loading for neurons with the highest motor index (M = 0.0105, SD = 0.0237) (i.e. the bin centered on 0.75) was significantly weaker than the mean loading for neurons with lower motor indices (bin centered on 0.25: M = 0.1539, SD = 0.2207; bin centered on 0: M = 0.1743, SD = 0.2429) (Figure 3B). Note that similar results were obtained when motor index was entered as a continuous variable into a multiple regression analysis instead of being discretized into four equally spaced bins (Figure 1 - figure supplement 1). The proportion of variance explained by the model, which also included subject name as a categorical variable to control for intersubject differences, was 0.0350 ($F(2, 368) = 6.6748$, $p = 0.0014$). Consistent with our hypothesis, we found that motor index was significantly associated with squared component loadings ($t = -3.6154$, $p = 0.0003$) such that SC neurons with a higher motor index explained less variance in the slow drift axis. These results demonstrate that even though arousal-related fluctuations are present in the SC, they are isolated from deep-layers neurons that elicit a strong saccadic response and presumably reside closer to the motor output. As a further test of this hypothesis, we next sought to determine if these same cells explained less variance in projections onto the PFC slow drift axis.

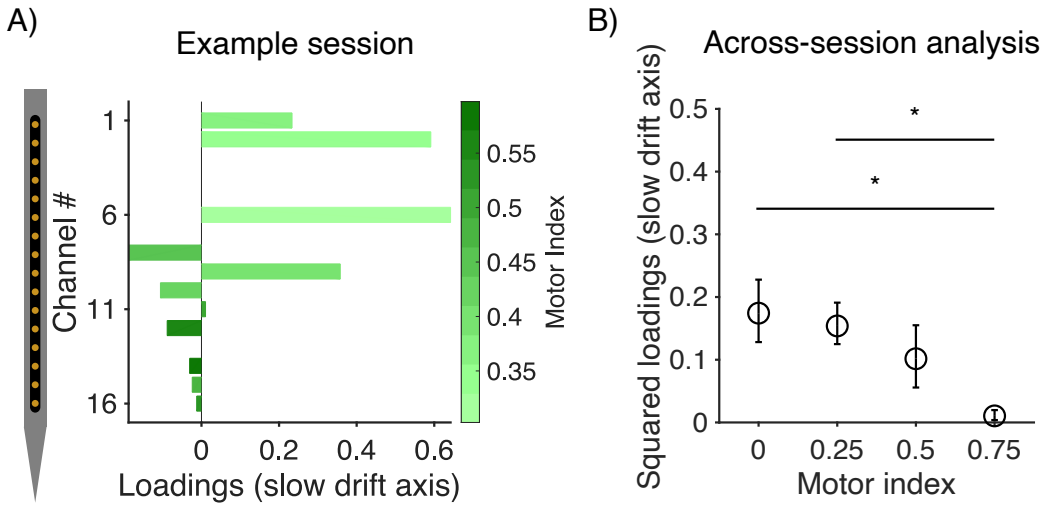

Figure 3. Arousal-related fluctuations are isolated from SC neurons with a higher motor index. (A) Loadings for the slow drift axis for an example session. Motor index is represented by the colorbar. Note that loadings were weaker for neurons recorded from channels at the bottom of the probe, which targeted neurons in the deep layers of the SC. These neurons also had higher motor indices, consistent with their role in eye movement generation. (B) Scatter plot for the across session analysis showing squared loadings for the slow drift axis pooled across all recorded SC neurons. The neurons were discretized into four equally spaced bins based on motor index, and permutation tests performed to investigate if neurons with a higher motor index explained less variance in the slow drift axis. The resultant p-values were then corrected for multiple comparisons using Bonferroni adjustment. $p < 0.05$*, $p < 0.01$**, $p < 0.001$***.

<u>SC neurons with a higher motor index are less correlated with the PFC slow drift axis</u>

To probe the relationship between deep-layer SC neurons and the PFC slow drift axis, we computed the correlation (Pearson's product-moment correlation coefficient) between the trial-to-trial residual responses of each SC neuron during the delay period and projections onto the PFC slow drift axis. Consistent with our finding that SC slow drift was significantly correlated with PFC slow drift (Figure 2B), we observed that the trial-to-trial residual responses of some SC neurons were significantly correlated with projections onto the PFC slow drift axis. For example, the residual responses of the neuron shown in Figure 4A, which has a relatively low motor index and is therefore unlikely to reside close to the motor output of the SC, were strongly correlated with projections onto the PFC slow drift axis ($r^2 = 0.5346$, $p < 0.001$). However, other neurons showed no correlation such as that in Figure 4B. The residual responses of this neuron, which has

a relatively high motor index and presumably resides closer to the motor output stage, were not significantly correlated with projections onto the PFC slow drift axis ($r^2 = 0.0010$, $p = 0.2650$).

To explore if a similar effect was found across sessions, we again pooled the motor indices of all recorded SC neurons and discretized them into four equally spaced bins. We performed permutation tests across the bins to investigate if the mean variance explained between residual SC neuron responses and projections onto the PFC slow drift axis was lower for neurons with a higher motor index. After controlling for multiple comparisons, we found that the mean variance explained was significantly lower for neurons with the highest motor index SC (M = 0.0209, SD = 0.0236) (i.e. the bin centered on 0.75) than it was for neurons with lower motor indices (bin centered on 0.25: M = 0.1240, SD = 0.1468; bin centered on 0: M = 0.1557, SD = 0.1591) (Figure 4C). Furthermore, the mean variance explained for neurons with an intermediate motor index (i.e. the bin centered on 0.5) (M = 0.0703, SD = 0.1095) was significantly lower than it was for neurons with the lowest motor indices (i.e. the bins centered on 0.25 and 0). Once again, similar results were obtained when the motor index was entered as a continuous variable into a multiple regression model instead of being discretized into bins (Figure 1 - figure supplement 1). The proportion of variance explained by the model, after controlling intersubject differences, was 0.1777 ($F(2, 368) = 39.7739$; $p < 0.001$). Motor index was significantly associated with the strength of the relationship between single SC neurons responses and projections onto the PFC slow drift axis ($t = -2.7902$; $p = 0.0055$) such that it was weaker for neurons with a higher motor index. These findings provide additional support for the hypothesis that arousal-related fluctuations are isolated from neurons in the deep layers of the SC. They are more characteristic of cells residing at the early to mid stages of the visuomotor transformation, which have been implicated in autonomic processes such as controlling the size of the pupil (Wang et al., 2012; Wang and Munoz, 2018).

This prompted us to ask if a relationship exists between SC neurons responses and pupil size, and whether this relationship is mediated by motor index.

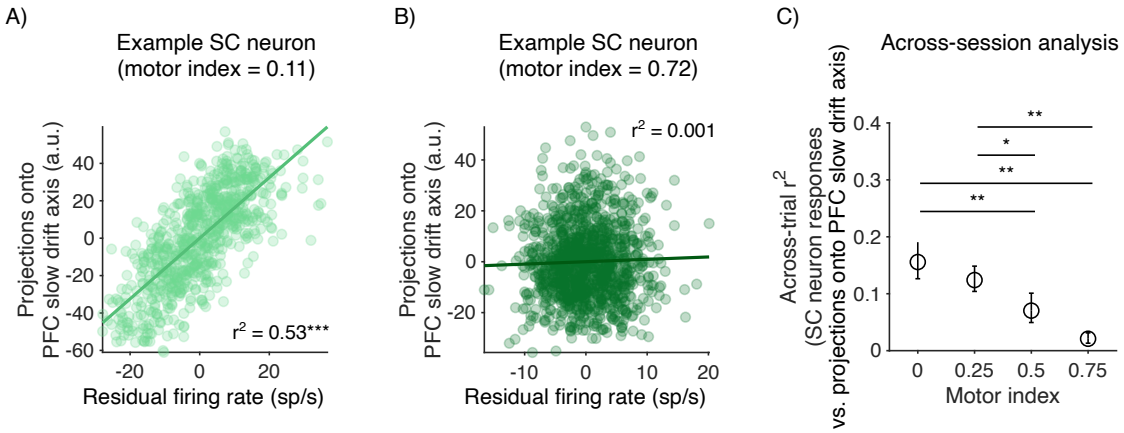

Figure 4. SC neurons with a higher motor index are less correlated with the PFC slow drift axis. (A) Example SC neuron with a relatively low motor index that exhibited a significant correlation between its residual spiking response and projections onto the PFC slow drift axis ($r^2 = 0.5346$, $p < 0.001$). (B) Example SC neuron with a relatively high motor index that did not exhibit a correlation between its residual spiking response and projections onto the PFC slow drift axis ($r^2 = 0.001$, $p = 0.2650$). (C) Scatter plot for the across session analysis showing the mean variance explained between residual spiking responses and projections onto the PFC slow drift axis for all recorded SC neurons. The neurons were discretized into four equally spaced bins based on motor index, and permutation tests performed to investigate if the variance explained between residual SC spiking responses and projections onto the PFC slow drift was lower for neurons with a higher motor index. The resultant p-values were then corrected for multiple comparisons using Bonferroni adjustment. $p < 0.05$*, $p < 0.01$**, $p < 0.001$***.

The relationship between SC neuron responses and pupil size is modulated by motor index

Previous work has shown that intermediate-layer SC neurons control the size of the pupil via: 1) direct projections to the Edinger-Westphal nucleus; and 2) indirect projections to the mesencephalic cuneiform nucleus (Joshi and Gold, 2020). Thus, we hypothesized that neurons with a lower motor index would explain more variance in trial-to-trial pupil size than neurons in deep layers. To test this, we computed the correlation (Pearson's product-moment correlation coefficient) between the spiking responses of each SC neuron and pupil size, both of which were computed during the first 200ms of the delay period. In several sessions, we found that the strength of this relationship was inversely related to motor index. For example, the spiking response of the

422 neuron shown in Figure 5A, which has a relatively low motor index and presumably resides at the
423 mid stage of the visuomotor transformation, was strongly correlated with pupil size ($r^2 = 0.2121$,
424 $p < 0.001$). In contrast, the spiking responses of the neuron shown in Figure 5B, which has a
425 relatively high motor index and presumably resides closer to the motor output stage, was not
426 significantly correlated with changes in pupil size over the course of a recording session ($r^2 =$
427 0.001, $p = 0.7534$).

428 To determine if a similar effect was found across sessions, we performed a multiple
429 regression analysis. In this analysis, we sought to determine if motor index predicted the strength
430 of the relationship between SC neuron responses during the delay period and pupil size, as
431 measured using the coefficient of determination (r^2). After controlling for intersubject differences,
432 results showed that the proportion of variance explained by the model was 0.0309 ($F(2, 368) =$
433 5.8717; $p = 0.0031$). Motor index was significantly associated with the strength of the relationship
434 between SC neuron responses and pupil size ($t = -3.2593$; $p = 0.0012$) (Figure 5C). More
435 specifically, we found a stronger relationship between neuronal response and pupil size for neurons
436 with a lower motor index, consistent with the proposed role of intermediate-layer SC neurons in
437 controlling the size of the pupil (Joshi and Gold, 2020).

438 We also considered whether shifts in SC neural activity could be driven directly by changes
439 in luminance induced by changes in the size of the pupil. If such luminance sensitivity existed in
440 SC among the visually selective neurons, it could explain the slow fluctuations in their activity
441 correlating with slow fluctuations in the size of the pupil. To ask whether this might be the case,
442 we performed two analyses. First, we analyzed the pupil size in a different period of time, the
443 baseline period before target presentation. Although there was only a fixation point on the screen
444 at that time and no target to induce a transient visual response to luminance, we found similar

445 results relating SC spiking responses to pupil size (Figure 5 - figure supplement 1). Second, we
446 compared slow drift measures computed on spiking responses during different epochs, and found
447 they were highly correlated (FIGURE 2 – figure supplement 1). Because slow drift is computed
448 on an average spiking across many trials, this makes it unlikely that transient luminance-induced
449 responses could lead to changes in these fluctuations. In our previous work, we also found that
450 slow drift occurred on a timescale of minutes in conjunction with changes in pupil size (Cowley
451 et al., 2020) and were correlated with eye measures such as reaction time, saccadic velocity and
452 microsaccade rate (Johnston et al., 2022a). Together, these analyses and previous results make
453 luminance changes induced by shifts in pupil size an unlikely explanation for slow fluctuations in
454 the firing of visually-responsive neurons in SC.

455 Taken together, the findings outlined above suggest that arousal-related signals are kept
456 separate from neurons in the deep layers of the SC. In addition to being more weakly correlated
457 with pupil size, the spiking responses of these neurons did not exhibit large fluctuations over time
458 (Figure 2), and when considering the neuronal population as a whole, explained less variance in
459 the slow drift axis when it was computed using population activity in the SC (Figure 3) and PFC
460 (Figure 4). Although these results point to a segregation of arousal- and eye movement-related
461 signals in the SC, research has shown that all three layers receive input from the LC: a brain region
462 that has long been associated with controlling global arousal levels (Benavidez et al., 2021). Thus,
463 an additional mechanism may have evolved to ensure that arousal-related signals are kept separate
464 from those used in the encoding of eye position. In primary motor cortex, signals related to
465 movement preparation reside in an orthogonal axis in population activity space to those that are
466 used for movement initiation so that they do not lead to premature muscle contractions (Kaufman

et al., 2014; Elsayed et al., 2016). Next, we explored if a similar mechanism exists in the SC to prevent arousal-related signals interfering with the motor output.

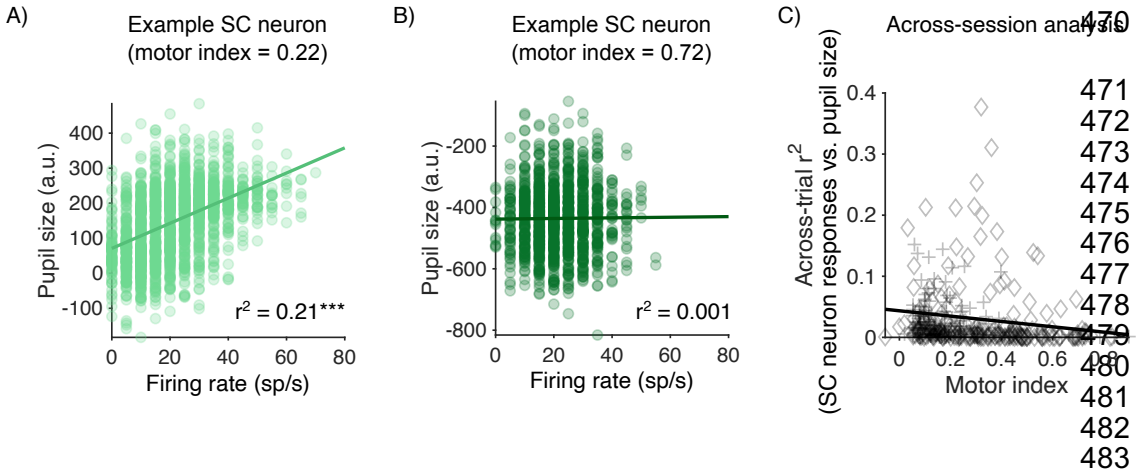

Figure 5. The relationship between SC neuron responses and pupil size is modulated by motor index. (A) Example SC neuron with a relatively low motor index that exhibited a significant correlation between its spiking response and pupil size. (B) Example SC neuron with a relatively high motor index that did not exhibit a correlation between its spiking response and pupil size ($r^2 = 0.1601$, $p < 0.001$). (C) Scatter plot showing that the strength of the relationship between individual SC neuron responses and pupil size is inversely related to motor index ($r^2 = 0.0309$, $p = 0.0031$). $p < 0.05$*, $p < 0.01$**, $p < 0.001$***.

<u>Arousal-related signals in the SC reside in an orthogonal subspace to saccade-related signals</u>

To investigate if arousal-related signals in the SC reside in an orthogonal subspace to those that are used to encode eye position, we computed a "pupil size axis" for each session. We discretized trial-to-trial pupil size into eight equally spaced bins and, for each neuron, computed the mean spiking response per bin (Figure 6A, left). We then used PCA to find the axis in population activity space that explained the most variance in the data attributable to the pupil. The loadings (Figure 6A, right) represent the correlation between the response of each neuron across bins and the first principal component meaning that neurons exhibiting a stronger relationship between firing rate and pupil size (e.g. Figure 6A, Channel 5) explained more variance in the pupil

size axis. Our goal was to compare projections onto the pupil size axis to projections onto a "saccade tuning axis". To compute this axis, tuning curves were generated for each SC neuron by taking the mean spiking response during the saccade epoch for each target angle (Figure 6B, right). PCA was then applied to the tuning curves, which yielded a vector of loadings for the first principal component (Figure 6B, left). In this case, neurons that exhibited greater selectivity for a particular target angle explained more variance in the saccade tuning axis (e.g. Figure 6B, Channel 11).

We first investigated if the pupil size axis and the saccade tuning axis reside in orthogonal subspaces. To ensure that fair comparisons could be made, the same data (i.e. trial-to-trial residual responses during the delay period) were projected onto each of the axes. We then computed a correlation (Pearson's product-moment correlation coefficient) between the projection values for each session, and used the coefficient of determination (r^2) to assess the variance explained. If arousal-related signals in the SC reside in an orthogonal subspace to those that are used for saccade generation, one would expect projections onto the pupil size axis to be weakly correlated with projections onto the saccade tuning axis. This was found to be the case in several sessions such as that shown in Figure 6C ($r^2 = 0.0307$, $p < 0.001$). Furthermore, when the data were pooled across sessions, we found that the mean variance explained between the projection values was 0.5142 (Figure 6D). By comparing the actual distribution of r^2 values to a null distribution that was generated by correlating projections onto the pupil size axis with projections onto an axis that was randomly oriented in population activity space, we were able to show that the mean variance explained was not significantly greater than what would be expected for data projected onto a random axis ($p = 0.5192$).

Finally, as an additional test of our hypothesis, we investigated if the pupil size axis was more aligned to the slow drift axis than the saccade tuning axis. To do this, we projected trial-to-

trial residual responses during the delay period onto the pupil size axis and the saccade tuning axis. For each session, we then correlated (Pearson's product-moment correlation coefficient) these projection values with projections onto the slow drift axis. Across sessions, we found that the mean variance explained between projections onto the pupil size axis and the slow drift axis ($M = 0.7780$, $SD = 0.3025$) was significantly greater than the mean variance explained between projections onto the saccade tuning axis ($M = 0.5319$, $SD = 0.3407$) ($t = -4.8578$, $p < 0.001$).

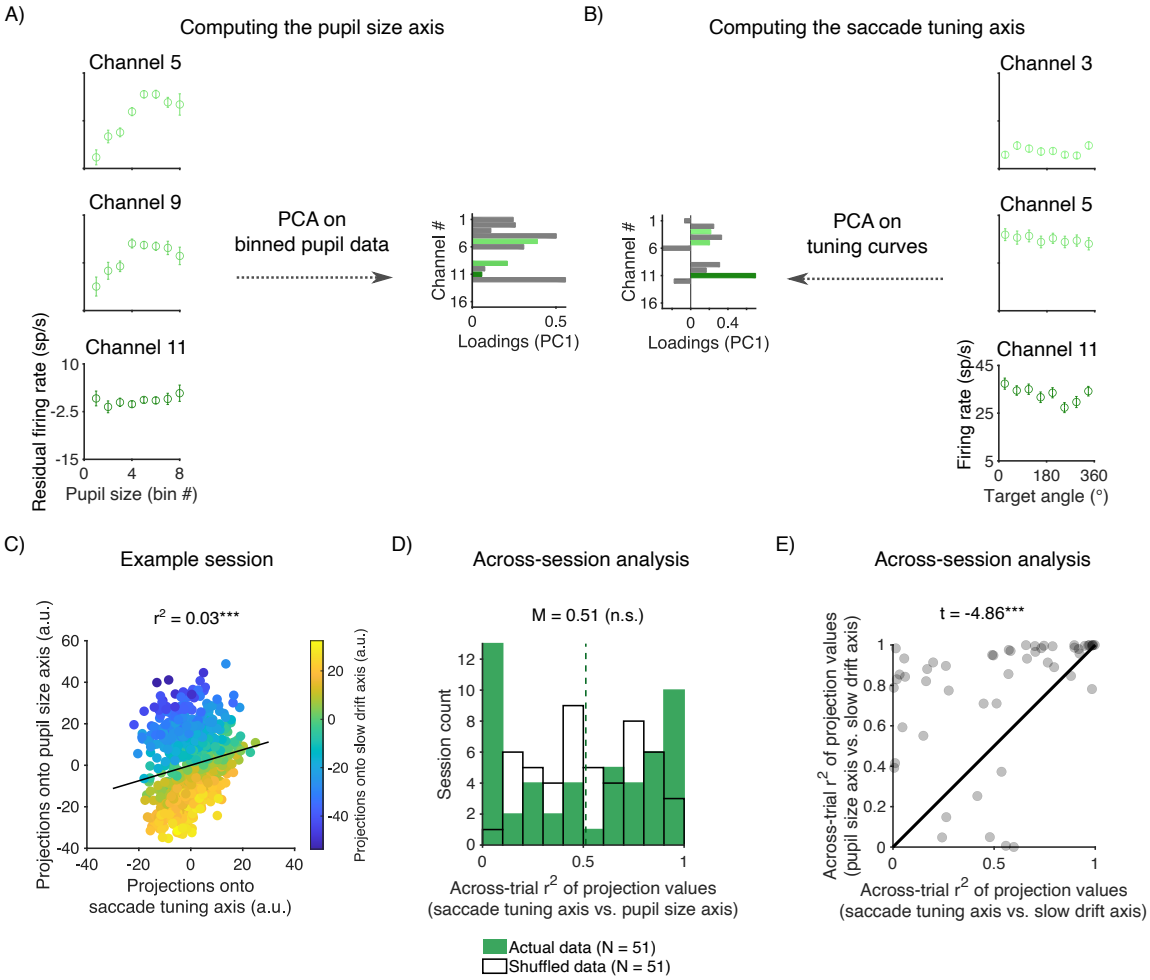

Figure 6. Arousal-related signals in the SC reside in an orthogonal subspace to saccade-related signals. (A) Computing the pupil size axis for an example session. Three example SC neurons from the same recording session (left). Each data point represents the mean spiking response after trial-to-trial pupil size had been discretized into eight equally spaced bins. Note that pupil size increases with bin number such that bin 1 contains trials in which the pupil was most constricted, whereas bin 8 contains trials in which the pupil was most dilated When PCA was applied to the data it yielded a vector of loadings for the first principal component (right). (B) Computing the saccade tuning axis for the same session shown in (A). Three example SC neurons (right). Each point represents the mean spiking response during the saccade epoch (25ms before to 25ms after the onset of the saccade) for each target angle. When PCA was applied to the data it yielded a vector of loadings for the first principal component (left). (C) A scatter plot showing the relationship between projections onto the pupil size axis and the saccade tuning axis for the same example session shown in (A) and (B). The color scale represents projections onto the slow drift axis. Note that the same data (i.e. residual SC responses during the delay period) were projected onto the three axes. (D) Histogram showing the proportion of variance explained between projections onto the pupil size axis and projections onto the saccade tuning axis. A p-value was computed by comparing the actual distribution of values to a null distribution (see Methods). (E) Scatter plot comparing the variance explained between projections onto the pupil size axis and the slow drift axis, and projections onto the saccade tuning axis and the slow drift axis. A p-value was computed using a paired-sample t-test. $p < 0.05$*, $p < 0.01$**, $p < 0.001$***.

557 Discussion

558 The main aim of this study was to identify how global fluctuations in arousal affect
559 subcortical areas like the SC, and how such fluctuations interact with the motor functions of that
560 area. In addition to representing a highly conserved brain structure in vertebrates, evidence
561 suggests that the SC also has a number of divergent properties that have been linked to higher-
562 order cognitive processes such as spatial attention (Knudsen, 2011; Krauzlis et al., 2013; Clark et
563 al., 2015; Basso et al., 2021) and perceptual decision-making (Ratcliff et al., 2003; Horwitz et al.,
564 2004; Crapse et al., 2018; Jun et al., 2021). In a similar way to how cortical motor areas separate
565 out preparatory signals (Kaufman et al., 2014; Elsayed et al., 2016) and signals from the opposing
566 arm (Ames and Churchland, 2019) when performing a reach movement, oculomotor structures
567 such as the SC must be able to disentangle signals related to cognition and brain state from those
568 used for eye movement encoding.

569 Consistent with what has been observed in the cortex (Cowley et al., 2020), we found that
570 the activity of some SC neurons fluctuated over time, and by reducing the dimensionality of the
571 data we were able to isolate a neuronal signature of arousal that was correlated with pupil size and
572 simultaneously recorded PFC data. In the context of the SC, this motivated us to ask how the
573 precise coordination of saccades is maintained despite the presence of ongoing fluctuations in brain
574 state. Another internal cognitive state that has been studied in the context of the visual and motor
575 role of the SC is spatial attention. Research using single-unit recordings in monkeys
576 (Ignashchenkova et al., 2004) and neuroimaging in humans (Katyal et al., 2010) has shown that
577 the effects of spatial attention on SC activity are layer-specific and more characteristic of neurons
578 in the superficial and intermediate layers. At a population level, attention has been shown to
579 increase the efficacy of communication from MT to SC in a similar manner for visual and motor

580 SC populations (Srinath et al., 2021) and reshape the visual information provided by MT to SC
581 (Ruff and Cohen, 2019). Overall, both spatial attention and global arousal share the property of
582 having an influence on the eye movement system while at the same time needing to avoid directly
583 producing unwanted eye movements. Here, we propose that arousal-related signals in the SC are
584 segregated from the motor planning function of SC to prevent unwanted changes in eye position.

585 To test this hypothesis, we utilized linear array recordings to simultaneously monitor the
586 activity of SC neurons with distinct neurophysiological response properties (Massot et al., 2019;
587 Ayar et al., 2023). Across sessions, we found that neurons exhibiting a stronger saccadic response,
588 which largely reside in the deep layers of the SC closer to the motor output (Basso and May, 2017),
589 were less connected to SC slow drift measured in the population response. Furthermore, by
590 correlating the response of these cells with a slow drift axis that was generated using
591 simultaneously recorded PFC data, we were able verify the global nature of this signal. These
592 findings are consistent with neuroimaging studies showing that changes in brain state lead to
593 coordinated fluctuations of activity across the brain (Liu et al., 2018; Turchi et al., 2018; Setzer et
594 al., 2022), and research that recorded simultaneously from neurons in cortical areas and subcortical
595 areas such as the LC (Joshi and Gold, 2022; Collins et al., 2023). Furthermore, our results suggest
596 that arousal-related fluctuations are more characteristic of neurons residing in the intermediate
597 layers of the SC. In support of this, several studies have pointed to a link between the activity of
598 these cells and non-invasive markers of arousal such as pupil size (Wang et al., 2012, 2014; Joshi
599 et al., 2016; Wang and Munoz, 2021).

600 To further study the role of intermediate-layer SC neurons in controlling the size of the
601 pupil, we investigated if the strength of the relationship between trial-to-trial changes in pupil size
602 and SC spiking responses was mediated by motor index. Consistent with the proposed link between

603 intermediate-layer neurons and pupil size, we found that cells exhibiting a weaker saccadic
604 response explained more variance in pupil size than neurons with a stronger saccadic response.
605 These results provide further support for the notion that arousal-related signals are kept separate
606 from signals used to encode eye position in the SC. This provides a potential mechanism through
607 which signals related to cognition and brain state can exist in oculomotor structures without
608 affecting high precision fixation and eye movements.

609 In addition to being kept separate at the level of different layers in the SC, signals related
610 to arousal and eye position encoding may also occupy different dimensions in population activity
611 space. The term "subspace" is often used when referring to the fact that the activity of
612 simultaneously recorded neurons is correlated (Cohen and Kohn, 2011) and occupies fewer
613 dimensions than the number of neurons in the population (Ebitz and Hayden, 2021; Rust and
614 Cohen, 2022). The concept of a subspace has been used to identify how populations of neurons
615 segregate different types of activity at the population level, rather than simply in different neurons.
616 Non-overlapping subspaces can be used to encode different types of sensory information (Mante
617 et al., 2013; Aoi et al., 2020; Ebitz et al., 2020), facilitate communication between distinct neural
618 circuits (Semedo et al., 2019, 2022), and isolate preparatory signals from movement commands
619 (Churchland and Shenoy, 2024). For example, when recording from neurons in the motor cortex
620 while monkeys performed a delayed-reach task, (Kaufman et al., 2014) found that preparatory
621 signals reside in an orthogonal subspace to those used to encode reach direction. In the SC, (Ayar
622 et al., 2023) found that signals related to sensation and action occupy separate subspaces and
623 depend upon the cognitive demands of the task, consistent with previous research showing that the
624 temporal structure of the SC population response differs during visual and motor epochs (Jagadisan
625 and Gandhi, 2022). To explore if a similar mechanism exists in the SC, we projected trial-to-trial

responses onto a pupil size axis and a saccade encoding axis, and found that the variance explained was not significantly greater than what would be expected for data projected onto a random axis. Furthermore, projections onto the pupil size axis were more aligned to projections onto the slow drift axis than projections onto the saccade encoding axis. Taken together, these findings suggest that arousal-related signals reside in an orthogonal subspace to those used to encode eye movement plans. In a similar manner to how preparatory signals in the motor cortex do not lead to premature muscle contractions (Kaufman et al., 2014; Elsayed et al., 2016), this might explain why arousal-related signals in the SC do not lead to unwanted changes in eye position.

In summary, by simultaneously recording from populations of neurons in the SC and the PFC, we were able to observe a fluctuation of activity that was present in both areas and correlated with non-invasive markers of arousal such as pupil size. The presence of arousal-related signals in the SC is consistent with its role in cognitive processes such as spatial attention and decision-making. However, it also raises the question of how motor areas can disentangle these higher-order signals from those used for movement encoding. In addition to being kept separate at the level of different layers in the SC, our results demonstrate that signals related to arousal and eye movement planning occupy distinct dimensions in population activity space. Further research is needed to determine whether this represents a similar mechanism to that which is used in the motor cortex to separate preparatory signals from movement commands (Churchland and Shenoy, 2024). If so, it could provide an explanation for how cognitive signals can be intermixed and impact activity in populations of SC neurons without affecting precision in fixation and saccadic eye movements.

Methods

649 Subjects

650 Two adult rhesus macaque monkeys (Macaca mulatta) were used in this study (Monkey
651 Do = 28 sessions, Monkey Wa = 34 sessions). Surgical procedures to chronically implant a
652 titanium head post (to immobilize the subjects' heads during experiments) and microelectrode
653 arrays were conducted in aseptic conditions under isoflurane anesthesia. Recording chambers
654 situated along the midline at an angle of 30° from vertical and aimed at a location 8mm above
655 interaural zero were also implanted for SC recordings. Opiate analgesics were used to minimize
656 pain and discomfort during the perioperative period. Experimental procedures were approved by
657 the Institutional Animal Care and Use Committee of Carnegie Mellon University and were
658 performed in accordance with the United States National Research Council's Guide for the Care
659 and Use of Laboratory Animals.

660

661 Superior colliculus (SC) recordings

662 The spiking responses of neuronal populations in the SC were recorded using a 16-channel
663 linear microelectrode array (V-Probe, Plexon, Dallas, TX). The total length of the linear array was
664 115mm. The contacts were spaced 150μm apart and spanned a distance of 2.25mm. Linear arrays
665 were lowered into the SC through a guide tube using a custom-designed mechanical microdrive
666 (Laboratory for Sensorimotor Research, Bethesda, MD), which was inserted through a plastic grid
667 with 1mm spacing.

668

669 Prefrontal cortex (PFC) recordings

670 The spiking responses of neuronal populations in the PFC (Monkey Do = left hemisphere,
671 Monkey Wa = right hemisphere) were recorded using 96-channel "Utah" arrays (Blackrock

672 Microsystems). The arrays comprised a 10x10 grid of silicon microelectrodes (1mm in length) that
673 were spaced 400µm apart, implanted on the pre-arcuate gyrus (8Ar).
674
675 Waveform classification
676 Signals from the linear probes (SC) and Utah arrays (PFC) were amplified and band-pass
677 filtered (0.3–7500Hz) by a Grapevine system (Ripple). Waveform segments crossing a threshold
678 (set as a multiple of the root mean square noise on each channel) were digitized (30KHz) and
679 stored for offline processing, which involved waveforms being automatically sorted as spikes or
680 noise by a neural network classifier developed in our laboratory (code available at
681 https://github.com/smithlabvision/spikesort/nasnet). Although this method cannot distinguish
682 between multiple neurons recorded from the same channel, it provides fast and accurate
683 classifications that are highly similar to those of a human spike-sorter (Issar et al., 2020). All
684 waveforms recorded from a single channel that remained after the neural network classifier had
685 been applied were considered to be from a single unit, which we refer to as a "neuron".
686
687 Exclusion criteria
688 Across both monkeys, we recorded from 992 sites in SC and 5952 sites in PFC. This
689 included all channels from the 16-channel linear microelectrode array and all channels from the
690 96-channel utah array across all sessions (SC: Monkey Do = 448, Monkey Wa = 544; PFC:
691 Monkey Do = 2688, Money Wa = 3264). We applied a rigorous set of exclusion criteria designed
692 to eliminate neurons with noisy or unstable waveforms, those with low firing rates, and neurons
693 that did not have an evoked response during either the visual or motor epoch of the MGS

To identify candidate neurons that were mostly classified as containing noise waveforms by the neural network classifier, and therefore only comprised a small number of waveforms, we removed neurons that had a mean firing rate less than 2sp/s across the entire session (Smith and Sommer, 2013). This was calculated by taking the total number of spikes in the recording session from the beginning (before the task was started) to the end (after the last trial of the day), and dividing by the total time (including periods of task performance and periods outside of the trial). In addition to removing neurons that had a low mean firing rate across an entire session, we also removed SC neurons that did not exhibit elevated firing rates during the visual and motor epochs of the MGS tasks i.e. following the presentation of the target stimulus and during the onset of a saccade. This was quantified by computing a visual and motor index for each SC neuron (see below). Neurons were removed if the value of both of these indices was less than 0.05, indicating a lack of response during both epochs. To rule out the possibility that slow drift arose due to recording instabilities (e.g. the distance between the neuron and the microelectrode(s) changing over time), we only included neurons with stable waveform shapes throughout a session. Neurons were removed if they had a percent waveform variance greater than 10% (Cowley et al., 2020). We also removed neurons that exhibited abrupt changes in activity during a recording session. This was quantified by dividing each session into 20 non-overlapping time bins and computing the mean spike count per bin (Cowley et al., 2020). Neurons were removed if the change in activity between any two consecutive time bins was greater than 25% of the maximum activity of that neuron. Adopting these exclusion criteria ensured that slow drift did not arise due to recording instabilities. We also note that if drift were to occur due to recording instabilities, it would not be expected to affect neurons from the same penetration differentially based on their motor index (e.g., Figure 3A).

717 In order to obtain a precise estimate of the slow drift axis, and after controlling for low
718 firing rate and recording instabilities, we removed sessions that contained less than two SC or PFC
719 neurons (Monkey Do = 3 sessions, Monkey Wa = 5 sessions). Furthermore, we removed sessions
720 if they had a duration lasting less than 45 minutes (Monkey Do = 0 sessions, Monkey Wa = 3
721 sessions). Adopting these additional criteria ensured that there were enough variables and
722 observations to perform PCA and accurately compute the slow drift axis. Using all of this criteria,
723 the total number of sessions included in the analysis for Monkey Do and Monkey Wa was 25
724 sessions (SC = 190 neurons, PFC = 795) and 26 sessions (SC = 181, PFC = 2110), respectively.
725
726 Visual stimuli
727 Visual stimuli were generated using a combination of custom software written in
728 MATLAB (The MathWorks) and Psychophysics Toolbox extensions (Brainard, 1997; Pelli, 1997;
729 Kleiner et al., 2007). They were displayed on a CRT monitor (resolution = 1024 X 768 pixels;
730 refresh rate = 100Hz), which was viewed at a distance of 57cm and gamma-corrected to linearize
731 the relationship between input voltage and output luminance using a photometer and look-up-
732 tables.
733
734 Memory-guided saccade task
735 Subjects fixated a central point (diameter = 0.18°) on the monitor to initiate a trial (Figure
736 1A). After fixating within a circular window (diameter: Monkey Do = 2.38°, Monkey Wa = 1.10°)
737 for 200ms, a target stimulus (diameter = 0.55°) was presented for 200ms at one of eight angles
738 separated by 45°. The eccentricity of the target stimulus was determined on a session-by-session
739 basis by applying low-amplitude microstimulation to contacts along the linear microelectrode

array to evoke saccadic eye movements. Target eccentricity was then set such that it matched the endpoints of evoked saccades. After the target stimulus had been presented, subjects were required to maintain fixation for a delay period. The duration of the delay period chosen at random on each trial from a uniform distribution spanning 600-1100ms. If steady fixation was maintained throughout the delay period, the central point was extinguished prompting the subjects to make a saccade to the remembered target location. The subjects had 500ms to initiate a saccade. To receive a liquid reward, the subjects' gaze had to be maintained within a circular window centered on the remembered target location (diameter: Monkey Do = 2.93°, Monkey Wa = 2.20° for the first 12 sessions and 3.01° for the remaining 22 sessions) for 100ms. In a subset of sessions, the target was briefly reilluminated, after the fixation point was extinguished and the saccade had been initiated, to aid in saccade completion.

Eye tracking

Eye position and pupil diameter were recorded monocularly at a rate of 1000Hz using an infrared eye tracker (EyeLink 1000, SR Research).

Microsaccade detection

Microsaccades were detected during the delay period and were defined as eye movements that exceeded a velocity threshold of 6 times the standard deviation of the median velocity for at least 6ms (Engbert and Kliegl, 2003) (Figure 2 - figure supplement 2). To prevent overshoots (i.e. fast, oppositely directed gaze shifts that occur shortly after a microsaccade) being treated as separate eye movements, we merged microsaccades that occurred within 50ms of each other (McCamy et al., 2015). Finally, we assessed the validity of our microsaccade detection method by

computing the correlation (Pearson's product-moment correlation coefficient) between the amplitude and peak velocity of detected microsaccades for each session. The mean correlation between these two variables across sessions was 0.7601 (SD = 0.0678) indicating that our detection algorithm was robust, as microsaccades fell on the main sequence (Zuber et al., 1965).

Characterizing the response properties of SC neurons

To characterize the neurophysiological response properties of individual SC neurons, we first visualized SC responses by computing PSTHs aligned to the onset of the target stimulus and the onset of the saccade to the remembered target location, respectively (Figure 1B). Firing rates were computed in 1ms bins, averaged across trials and smoothed using a Gaussian function (σ = 5ms).

To further quantify the strength of the saccadic response to the remembered target location, a motor index was computed for each neuron as follows:

$$Motor\ index = \frac{M - B}{M + B}$$

Where M represents the mean response during a peri-saccade epoch from 25ms before to 25ms after the onset of the saccade, and B represents the mean response during a baseline period defined as 100ms before the onset of the target stimulus. Higher motor index values are indicative of a stronger saccadic response relative to baseline, whereas lower values represent a weaker saccadic response relative to baseline. Note that we also computed a visual index for each neuron, which was only used for the purpose of excluding neurons that did not exhibit an evoked response during the MGS task (see above). The visual index was computed in the following manner:

$$Visual\ index = \frac{V - B}{V + B}$$

785

786 Where *V* represents the mean response during a peri-stimulus epoch spanning 25ms to 125ms after
787 the onset of the target stimulus, and *B* represents the mean response during a baseline period
788 defined as 100ms before the onset of the target stimulus.

789

790 Generating shuffled distributions

791 Variance explained by SC slow drift axis across sessions

792 To determine if the variance explained by the SC slow drift axis was significantly greater
793 than chance across sessions, the actual distribution of proportion variance explained values was
794 compared to a shuffled distribution (Figure 2A, top right). To generate this distribution, PCA was
795 performed on binned spike counts that had first been shuffled across trials (1000 iterations). We
796 then computed the mean variance explained by the first principal component across iterations,
797 which yielded a single shuffled value for each session. Finally, a p-value was computed by
798 calculating the proportion of values in the shuffled distribution that were greater than or equal to
799 the actual variance explained across sessions.

800 Relationship between SC slow drift axis and the PFC slow drift

801 To assess the significance of the relationship between projections onto the SC slow drift
802 axis and the PFC slow drift axis (Figure 2B), we randomly shuffled the two variables across
803 sessions and re-computed the correlations (1000 iterations). Differences in session length were
804 controlled for by truncating longer sessions such that they comprised the same number of data
805 points as the shorter session. A p-value was then computed by calculating the proportion of values
806 in the shuffled distribution that were greater than or equal to the actual variance explained across
807 sessions. Note that an identical method was used to determine if projections onto the SC slow drift

axis explained a significant amount of the variance in pupil size (Figure 2C) and microsaccade rate (Figure 2 - figure supplement 2).

Orthogonality of the pupil size axis and the saccade tuning axis

To determine if the pupil size axis and the saccade tuning axis reside in orthogonal subspaces, we computed the correlation between projections onto each axis and then compared the actual distribution of r^2 values across sessions to a shuffled distribution (Figure 6D). To generate this distribution, projections onto the pupil size axis were correlated with projections onto an axis that was randomly orientated in population activity space (1000 iterations). The latter was generated in a similar manner to the saccade tuning axis, the only difference being that tuning curves were computed for target angles that had been shuffled across trials. We then computed the mean variance explained across iterations, which yielded a single shuffled value for each session. Finally, a p-value was computed by calculating the proportion of values in the shuffled distribution that were greater than or equal to the actual variance explained across sessions.

Acknowledgments

The authors would like to thank Samantha Schmitt for assistance with surgery and data collection, Karen McCracken for assistance with animal care, and Dr. Katerina Acar for advice about task design and assistance with the mapping of the recording chamber. We would also like to thank Dr. Siddhartha Joshi and Dr. Neeraj Gandhi for providing expert guidance about chamber placement. M. S. was supported by NIH R01 EY029250 and NIH R01MH128393.

References

Allen KM, Lawlor J, Salles A, Moss CF (2021) Orienting our view of the superior colliculus: specializations and general functions. Curr Opin Neurobiol 71:119–126.

Ames KC, Churchland MM (2019) Motor cortex signals for each arm are mixed across hemispheres and neurons yet partitioned within the population response. Elife 8 Available at: http://dx.doi.org/10.7554/eLife.46159.

Aoi MC, Mante V, Pillow JW (2020) Prefrontal cortex exhibits multidimensional dynamic encoding during decision-making. Nat Neurosci 23:1410–1420.

Aston-Jones G, Cohen JD (2005) An integrative theory of locus coeruleus-norepinephrine function: adaptive gain and optimal performance. Annu Rev Neurosci 28:403–450.

Ayar EC, Heusser MR, Bourrelly C, Gandhi NJ (2023) Distinct context- and content-dependent population codes in superior colliculus during sensation and action. Proc Natl Acad Sci U S A 120:e2303523120.

Basso MA, Bickford ME, Cang J (2021) Unraveling circuits of visual perception and cognition through the superior colliculus. Neuron 109:918–937.

Basso MA, May PJ (2017) Circuits for Action and Cognition: A View from the Superior Colliculus. Annu Rev Vis Sci 3:197–226.

Benavidez NL et al. (2021) Organization of the inputs and outputs of the mouse superior colliculus. Nat Commun 12:4004.

Bohlen MO, Warren S, May PJ (2017) A central mesencephalic reticular formation projection to medial rectus motoneurons supplying singly and multiply innervated extraocular muscle fibers. J Comp Neurol 525:2000–2018.

Bowers NR, Gautier J, Lin S, Roorda A (2021) Fixational eye movements in passive versus active sustained fixation tasks. J Vis 21:16.

Brainard D (1997) The Psychophysics Toolbox. Spat Vis 10:433–436.

Breton-Provencher V, Sur M (2019) Active control of arousal by a locus coeruleus GABAergic circuit. Nat Neurosci 22:218–228.

Cang J, Savier E, Barchini J, Liu X (2018) Visual Function, Organization, and Development of the Mouse Superior Colliculus. Annu Rev Vis Sci 4:239–262.

Castellote JM, Kumru H, Queralt A, Valls-Solé J (2007) A startle speeds up the execution of externally guided saccades. Exp Brain Res 177:129–136.

Cerkevich CM, Lyon DC, Balaram P, Kaas JH (2014) Distribution of cortical neurons projecting to the superior colliculus in macaque monkeys. Eye Brain 2014:121–137.

Churchland MM, Shenoy KV (2024) Preparatory activity and the expansive null-space. Nat Rev Neurosci 25:213–236.

Clark K, Squire RF, Merrikhi Y, Noudoost B (2015) Visual attention: Linking prefrontal sources to neuronal and behavioral correlates. Prog Neurobiol 132:59–80.

Cohen MR, Kohn A (2011) Measuring and interpreting neuronal correlations. Nat Neurosci 14:811–819.

Collins L, Francis J, Emanuel B, McCormick DA (2023) Cholinergic and noradrenergic axonal activity contains a behavioral-state signal that is coordinated across the dorsal cortex. Elife 12 Available at: http://dx.doi.org/10.7554/eLife.81826.

Contadini-Wright C, Magami K, Mehta N, Chait M (2023) Pupil dilation and microsaccades provide complementary insights into the dynamics of arousal and instantaneous attention during effortful listening. J Neurosci 43:4856–4866.

Cowley BR, Snyder AC, Acar K, Williamson RC, Yu BM, Smith MA (2020) Slow Drift of Neural Activity as a Signature of Impulsivity in Macaque Visual and Prefrontal Cortex. Neuron 108:551-567.e8.

Crapse TB, Lau H, Basso MA (2018) A Role for the Superior Colliculus in Decision Criteria. Neuron 97:181-194.e6.

de Gee JW, Colizoli O, Kloosterman NA, Knapen T, Nieuwenhuis S, Donner TH (2017) Dynamic modulation of decision biases by brainstem arousal systems. Elife 6 Available at: http://dx.doi.org/10.7554/eLife.23232.

Di Stasi LL, Catena A, Cañas JJ, Macknik SL, Martinez-Conde S (2013) Saccadic velocity as an arousal index in naturalistic tasks. Neurosci Biobehav Rev 37:968–975.

Ebitz RB, Hayden BY (2021) The population doctrine in cognitive neuroscience. Neuron 109:3055–3068.

Ebitz RB, Tu JC, Hayden BY (2020) Rules warp feature encoding in decision-making circuits. PLoS Biol 18:e3000951.

Edwards SB, Ginsburgh CL, Henkel CK, Stein BE (1979) Sources of subcortical projections to the superior colliculus in the cat. J Comp Neurol 184:309–329.

Elsayed GF, Lara AH, Kaufman MT, Churchland MM, Cunningham JP (2016) Reorganization between preparatory and movement population responses in motor cortex. Nat Commun 7:13239.

Engbert R, Kliegl R (2003) Microsaccades uncover the orientation of covert attention. Vision Res 43:1035–1045.

Gandhi NJ, Katnani HA (2011) Motor functions of the superior colliculus. Annu Rev Neurosci 34:205–231.

Goldberg ME, Wurtz RH (1972) Activity of superior colliculus in behaving monkey. I. Visual receptive fields of single neurons. J Neurophysiol 35:542–559.

Hafed ZM, Hoffmann K-P, Chen C-Y, Bogadhi AR (2023) Visual Functions of the Primate Superior Colliculus. Annu Rev Vis Sci 9:361–383.

Hafed ZM, Yoshida M, Tian X, Buonocore A, Malevich T (2021) Dissociable Cortical and Subcortical Mechanisms for Mediating the Influences of Visual Cues on Microsaccadic Eye Movements. Front Neural Circuits 15:638429.

Hennig JA, Oby ER, Golub MD, Bahureksa LA, Sadtler PT, Quick KM, Ryu SI, Tyler-Kabara EC, Batista AP, Chase SM, Yu BM (2021) Learning is shaped by abrupt changes in neural engagement. Nat Neurosci 24:727–736.

Hikosaka O, Wurtz RH (1983) Visual and oculomotor functions of monkey substantia nigra pars reticulata. III. Memory-contingent visual and saccade responses. J Neurophysiol 49:1268–1284.

Horwitz GD, Batista AP, Newsome WT (2004) Representation of an abstract perceptual decision in macaque superior colliculus. J Neurophysiol 91:2281–2296.

Huerta MF, Kaas JH (1990) Supplementary eye field as defined by intracortical microstimulation: connections in macaques. J Comp Neurol 293:299–330.

Ignashchenkova A, Dicke PW, Haarmeier T, Thier P (2004) Neuron-specific contribution of the superior colliculus to overt and covert shifts of attention. Nat Neurosci 7:56–64.

Isa T, Marquez-Legorreta E, Grillner S, Scott EK (2021) The tectum/superior colliculus as the vertebrate solution for spatial sensory integration and action. Curr Biol 31:R741–R762.

Issar D, Williamson RC, Khanna SB, Smith MA (2020) A neural network for online spike classification that improves decoding accuracy. J Neurophysiol 123:1472–1485.

Jagadisan UK, Gandhi NJ (2022) Population temporal structure supplements the rate code during sensorimotor transformations. Curr Biol 32:1010-1025.e9.

Johnston R, Snyder AC, Khanna SB, Issar D, Smith MA (2022a) The eyes reflect an internal cognitive state hidden in the population activity of cortical neurons. Cereb Cortex 32:3331–3346.

Johnston R, Snyder AC, Schibler RS, Smith MA (2022b) EEG Signals Index a Global Signature of Arousal Embedded in Neuronal Population Recordings. eNeuro 9 Available at: http://dx.doi.org/10.1523/ENEURO.0012-22.2022.

Jolliffe IT, Cadima J (2016) Principal component analysis: a review and recent developments. Philos Trans A Math Phys Eng Sci 374:20150202.

Joshi S, Gold JI (2020) Pupil Size as a Window on Neural Substrates of Cognition. Trends Cogn Sci 24:466–480.

Joshi S, Gold JI (2022) Context-dependent relationships between locus coeruleus firing patterns and coordinated neural activity in the anterior cingulate cortex. Elife 11 Available at: http://dx.doi.org/10.7554/eLife.63490.

Joshi S, Li Y, Kalwani RM, Gold JI (2016) Relationships between Pupil Diameter and Neuronal

Activity in the Locus Coeruleus, Colliculi, and Cingulate Cortex. Neuron 89:221–234.

Jun EJ, Bautista AR, Nunez MD, Allen DC, Tak JH, Alvarez E, Basso MA (2021) Causal role for the primate superior colliculus in the computation of evidence for perceptual decisions. Nat Neurosci 24:1121–1131.

Kardamakis AA, Saitoh K, Grillner S (2015) Tectal microcircuit generating visual selection commands on gaze-controlling neurons. Proc Natl Acad Sci U S A 112:E1956-65.

Katnani HA, Gandhi NJ (2011) Order of operations for decoding superior colliculus activity for saccade generation. J Neurophysiol 106:1250–1259.

Katyal S, Zughni S, Greene C, Ress D (2010) Topography of covert visual attention in human superior colliculus. J Neurophysiol 104:3074–3083.

Kaufman MT, Churchland MM, Ryu SI, Shenoy KV (2014) Cortical activity in the null space: permitting preparation without movement. Nat Neurosci 17:440–448.

Kleiner M, Brainard D, Pelli D (2007) What's new in psychtoolbox-3? perception 36. In: Ref Type: Abstract.

Knudsen EI (2011) Control from below: the role of a midbrain network in spatial attention. Eur J Neurosci 33:1961–1972.

Ko H-K, Poletti M, Rucci M (2010) Microsaccades precisely relocate gaze in a high visual acuity task. Nat Neurosci 13:1549–1553.

Komatsu H, Suzuki H (1985) Projections from the functional subdivisions of the frontal eye field to the superior colliculus in the monkey. Brain Res 327:324–327.

Krauzlis RJ, Lovejoy LP, Zénon A (2013) Superior colliculus and visual spatial attention. Annu Rev Neurosci 36:165–182.

Li L, Feng X, Zhou Z, Zhang H, Shi Q, Lei Z, Shen P, Yang Q, Zhao B, Chen S, Li L, Zhang Y, Wen P, Lu Z, Li X, Xu F, Wang L (2018) Stress Accelerates Defensive Responses to Looming in Mice and Involves a Locus Coeruleus-Superior Colliculus Projection. Curr Biol 28:859-871.e5.

Liu X, de Zwart JA, Schölvinck ML, Chang C, Ye FQ, Leopold DA, Duyn JH (2018) Subcortical evidence for a contribution of arousal to fMRI studies of brain activity. Nat Commun 9:395.

Mante V, Sussillo D, Shenoy KV, Newsome WT (2013) Context-dependent computation by recurrent dynamics in prefrontal cortex. Nature 503:78–84.

Massot C, Jagadisan UK, Gandhi NJ (2019) Sensorimotor transformation elicits systematic patterns of activity along the dorsoventral extent of the superior colliculus in the macaque monkey. Commun Biol 2:287.

Mathôt S (2018) Pupillometry: Psychology, Physiology, and Function. J Cogn 1:16.

971 May PJ (2006) The mammalian superior colliculus: laminar structure and connections. Prog
972 Brain Res 151:321–378.

973 McCamy MB, Otero-Millan J, Leigh RJ, King SA, Schneider RM, Macknik SL, Martinez-Conde
974 S (2015) Simultaneous recordings of human microsaccades and drifts with a
975 contemporary video eye tracker and the search coil technique. PLoS One 10:e0128428.

976 Mohler CW, Wurtz RH (1976) Organization of monkey superior colliculus: intermediate layer
977 cells discharging before eye movements. J Neurophysiol 39:722–744.

978 Müller JR, Philiastides MG, Newsome WT (2005) Microstimulation of the superior colliculus
979 focuses attention without moving the eyes. Proceedings of the National Academy of
980 Sciences 102:524–529.

981 Munoz DP, Wurtz RH (1995) Saccade-related activity in monkey superior colliculus. I.
982 Characteristics of burst and buildup cells. J Neurophysiol 73:2313–2333.

983 Murphy PR, O'Connell RG, O'Sullivan M, Robertson IH, Balsters JH (2014) Pupil diameter
984 covaries with BOLD activity in human locus coeruleus. Hum Brain Mapp 35:4140–4154.

985 Parthasarathy HB, Schall JD, Graybiel AM (1992) Distributed but convergent ordering of
986 corticostriatal projections: analysis of the frontal eye field and the supplementary eye
987 field in the macaque monkey. J Neurosci 12:4468–4488.

988 Pelli DG (1997) The VideoToolbox software for visual psychophysics: transforming numbers
989 into movies. Spat Vis 10:437–442.

990 Perry VH, Cowey A (1984) Retinal ganglion cells that project to the superior colliculus and
991 pretectum in the macaque monkey. Neuroscience 12:1125–1137.

992 Plummer NW, Chandler DJ, Powell JM, Scappini EL, Waterhouse BD, Jensen P (2020) An
993 Intersectional Viral-Genetic Method for Fluorescent Tracing of Axon Collaterals Reveals
994 Details of Noradrenergic Locus Coeruleus Structure. eNeuro 7 Available at:
995 http://dx.doi.org/10.1523/ENEURO.0010-20.2020.

996 Qu J, Zhou X, Zhu H, Cheng G, Ashwell KWS, Lu F (2006) Development of the human superior
997 colliculus and the retinocollicular projection. Exp Eye Res 82:300–310.

998 Ratcliff R, Cherian A, Segraves M (2003) A comparison of macaque behavior and superior
999 colliculus neuronal activity to predictions from models of two-choice decisions. J
1000 Neurophysiol 90:1392–1407.

1001 Reimer J, McGinley MJ, Liu Y, Rodenkirch C, Wang Q, McCormick DA, Tolias AS (2016)
1002 Pupil fluctuations track rapid changes in adrenergic and cholinergic activity in cortex.
1003 Nat Commun 7:13289.

1004 Robinson DA (1972) Eye movements evoked by collicular stimulation in the alert monkey.
1005 Vision Res 12:1795–1808.

Ruff DA, Cohen MR (2019) Simultaneous multi-area recordings suggest that attention improves performance by reshaping stimulus representations. Nat Neurosci 22:1669–1676.

Rust NC, Cohen MR (2022) Priority coding in the visual system. Nat Rev Neurosci 23:376–388.

Sara SJ, Bouret S (2012) Orienting and reorienting: the locus coeruleus mediates cognition through arousal. Neuron 76:130–141.

Semedo JD, Jasper AI, Zandvakili A, Krishna A, Aschner A, Machens CK, Kohn A, Yu BM (2022) Feedforward and feedback interactions between visual cortical areas use different population activity patterns. Nat Commun 13:1099.

Semedo JD, Zandvakili A, Machens CK, Yu BM, Kohn A (2019) Cortical Areas Interact through a Communication Subspace. Neuron 102:249-259.e4.

Setzer B, Fultz NE, Gomez DEP, Williams SD, Bonmassar G, Polimeni JR, Lewis LD (2022) A temporal sequence of thalamic activity unfolds at transitions in behavioral arousal state. Nat Commun 13:5442.

Smith MA, Sommer MA (2013) Spatial and temporal scales of neuronal correlation in visual area V4. J Neurosci 33:5422–5432.

Sparks DL (1986) Translation of sensory signals into commands for control of saccadic eye movements: role of primate superior colliculus. Physiol Rev 66:118–171.

Sparks DL, Hartwich-Young R (1989) The deep layers of the superior colliculus. Rev Oculomot Res 3:213–255.

Sparks DL, Mays LE (1990) Signal transformations required for the generation of saccadic eye movements. Annu Rev Neurosci 13:309–336.

Srinath R, Ruff DA, Cohen MR (2021) Attention improves information flow between neuronal populations without changing the communication subspace. Curr Biol 31:5299-5313.e4.

Stanton GB, Goldberg ME, Bruce CJ (1988) Frontal eye field efferents in the macaque monkey: II. Topography of terminal fields in midbrain and pons. J Comp Neurol 271:493–506.

Suzuki DG, Pérez-Fernández J, Wibble T, Kardamakis AA, Grillner S (2019) The role of the optic tectum for visually evoked orienting and evasive movements. Proc Natl Acad Sci U S A 116:15272–15281.

Turchi J, Chang C, Ye FQ, Russ BE, Yu DK, Cortes CR, Monosov IE, Duyn JH, Leopold DA (2018) The Basal Forebrain Regulates Global Resting-State fMRI Fluctuations. Neuron 97:940-952.e4.

van den Brink RL, Pfeffer T, Donner TH (2019) Brainstem Modulation of Large-Scale Intrinsic Cortical Activity Correlations. Front Hum Neurosci 13:340.

Wang C-A, Boehnke SE, Itti L, Munoz DP (2014) Transient pupil response is modulated by contrast-based saliency. J Neurosci 34:408–417.

Wang C-A, Boehnke SE, White BJ, Munoz DP (2012) Microstimulation of the monkey superior colliculus induces pupil dilation without evoking saccades. J Neurosci 32:3629–3636.

Wang C-A, Munoz DP (2018) Neural basis of location-specific pupil luminance modulation. Proc Natl Acad Sci U S A 115:10446–10451.

Wang C-A, Munoz DP (2021) Coordination of Pupil and Saccade Responses by the Superior Colliculus. J Cogn Neurosci 33:919–932.

Wheatcroft T, Saleem AB, Solomon SG (2022) Functional Organisation of the Mouse Superior Colliculus. Front Neural Circuits 16:792959.

White BJ, Berg DJ, Kan JY, Marino RA, Itti L, Munoz DP (2017) Superior colliculus neurons encode a visual saliency map during free viewing of natural dynamic video. Nat Commun 8:14263.

Winterson BJ, Collewijn H (1976) Microsaccades during finely guided visuomotor tasks. Vision Res 16:1387–1390.

Wurtz RH, Albano JE (1980) Visual-motor function of the primate superior colliculus. Annu Rev Neurosci 3:189–226.

Wylie DRW, Gutierrez-Ibanez C, Pakan JMP, Iwaniuk AN (2009) The optic tectum of birds: mapping our way to understanding visual processing. Can J Exp Psychol 63:328–338.

Zénon A, Krauzlis RJ (2012) Attention deficits without cortical neuronal deficits. Nature 489:434–437.

Zuber BL, Stark L, Cook G (1965) Microsaccades and the velocity-amplitude relationship for saccadic eye movements. Science 150:1459–1460.

Supplementary information

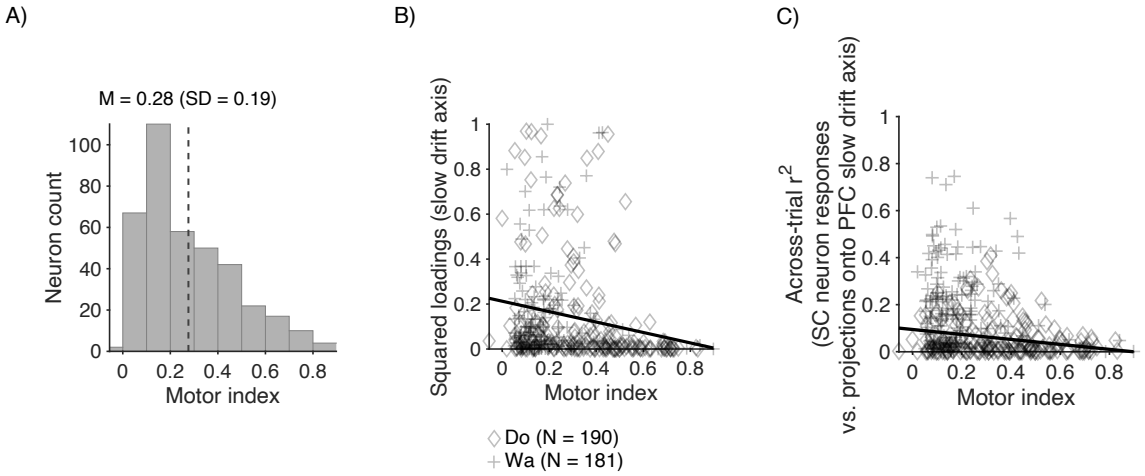

Figure 1 - figure supplement 1. (A) Histogram showing the distribution of motor index values computed across sessions for all recorded SC neurons. The mean value across sessions is denoted by the dashed line. (B) Scatter plot showing the relationship between motor index and squared component loadings for the SC slow drift axis. The line of best fit was computed using multiple regression. Motor index was entered as a continuous predictor variable along with subject name to control for differences between subjects. As described in the Results section, the model explained a significant amount of the variance in the data. A negative correlation was also found between motor index and squared loadings. (C) Scatter plot showing the relationship between motor index and the strength of the relationship between single SC neurons responses and projections onto the PFC slow drift axis, as measured by computing r^2. As in (B), the line of best fit was computed using multiple regression. Results showed that the model explained a significant amount of the variance in the data. Furthermore, a negative correlation was found between motor index and the r^2 between single neuron SC responses and projections onto the PFC slow drift axis.

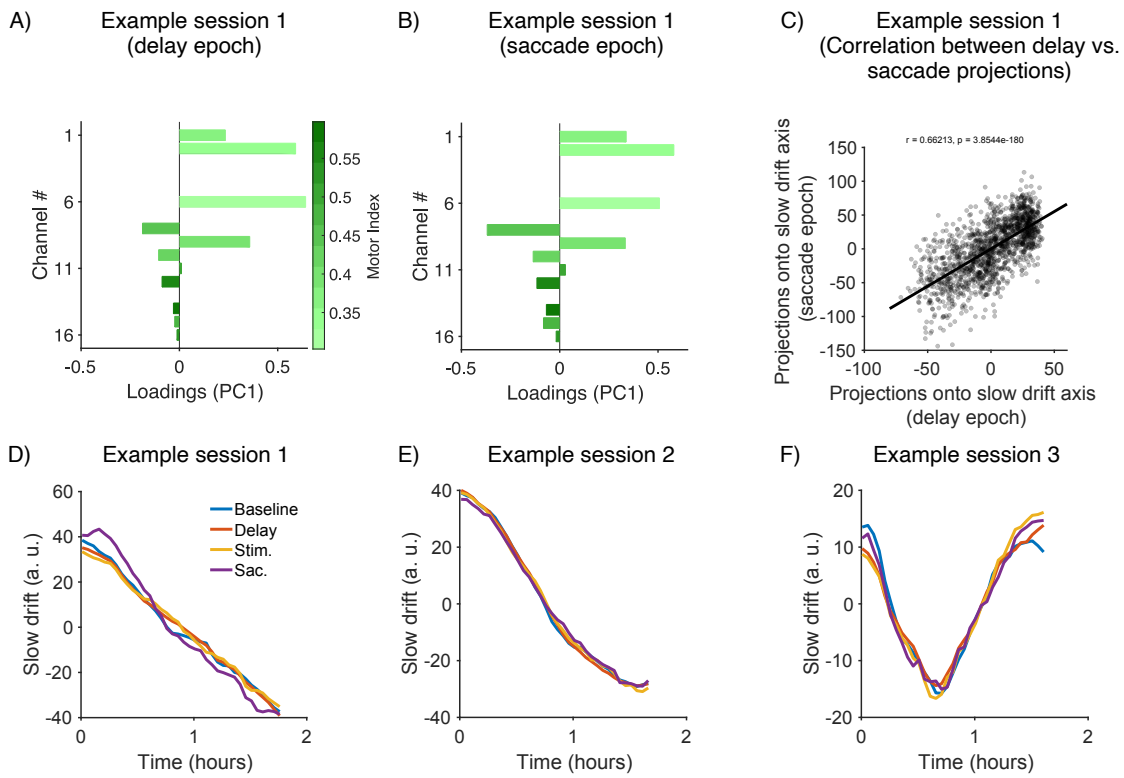

Figure 2 - figure supplement 1. (A) Loadings for the SC slow drift axis for an example session when it was computed using spiking responses during the delay period (same session as Figure 3A in main manuscript). (B) Loadings for the SC slow drift axis from the same session when it was computed using spiking responses during the saccade epoch. (C) Scatter plot showing the correlation between projections onto the slow drift axis for the same session when the slow drift axis was computed using spiking responses during the delay and saccade epochs (one data point per trial). (D-F) Dynamics of slow drift for three example sessions when the SC slow drift axis was computed using spiking responses during the baseline, delay, visual and saccade epochs. Note that the session in (D) is the same as that show in (A-C). Baseline = 100ms before the onset of the target stimulus; Delay = 600 to 1100ms after the offset of the target stimulus; Stim. = 25ms to 125ms after the onset of the target stimulus; Sac. = 25ms before to 25ms after the onset of the saccade.

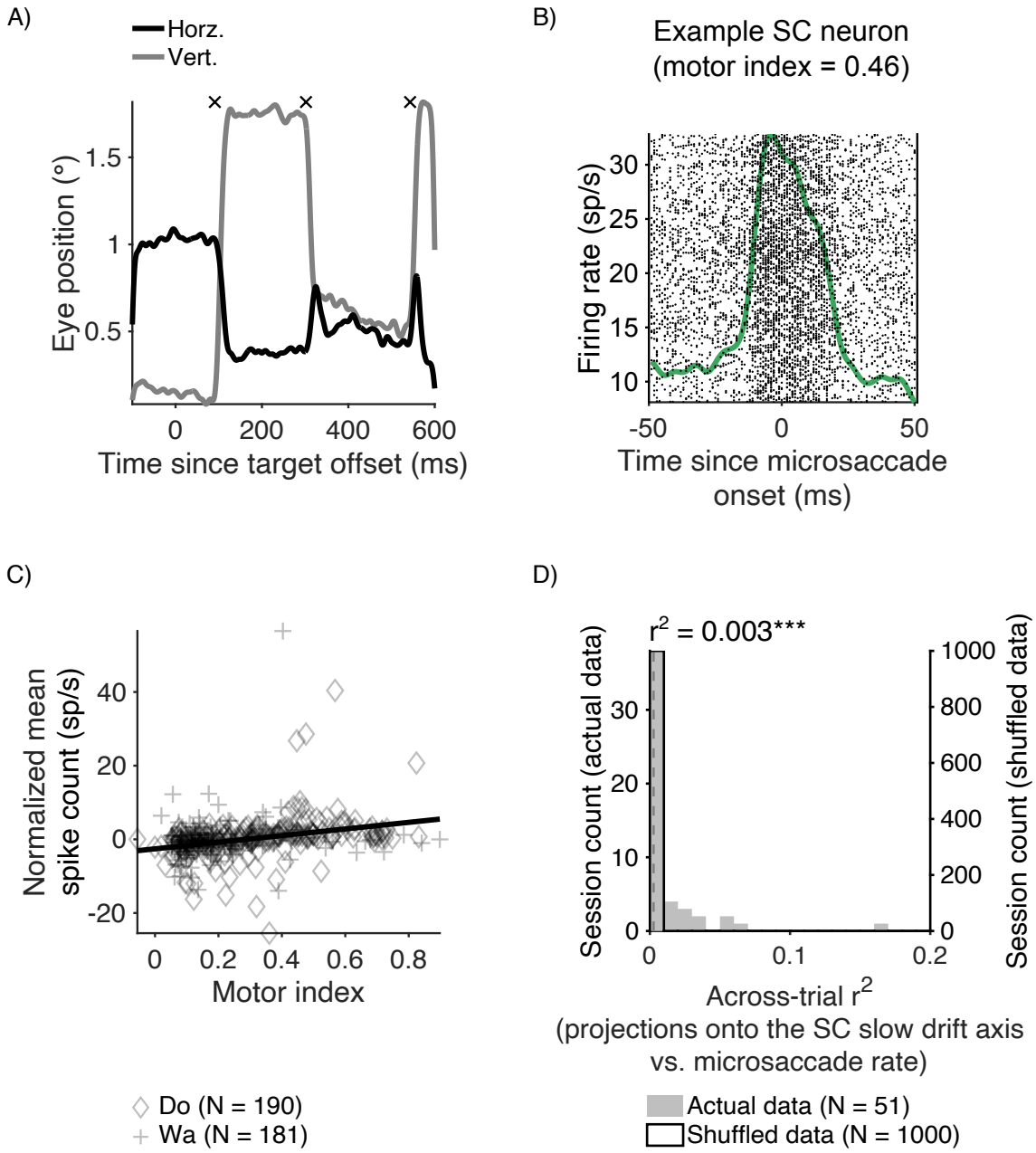

Figure 2 - figure supplement 2. (A) Horizontal and vertical eye position on a single trial during the MGS task. Microsaccades were detected using the delay period using a velocity-base algorithm (Engbert and Kliegl, 2003) and are indicated by black crosses. (B) PSTHs aligned to microsaccade onset. Firing rates were computed in 1ms bins, averaged across trials and smoothed using a Gaussian function (σ = 5ms). (C) Scatter plot showing the relationship between normalized mean firing rate in and around the time of a microsaccade and motor index for each recorded SC neuron. For each neuron, mean firing rates were computed in the period spanning 25ms before and 25m after a detected microsaccade, and were normalized by subtracting the mean activity across all trials during the same time period. This was done to control for the fact that some SC neurons (e.g. buildup neurons) have been found to increase their activity during the delay period on MGS tasks (Munoz and Wurtz, 1995). A multiple regression analysis was then performed to determine if normalized mean firing rate was associated with motor index. Results showed that the proportion of variance explained by the model, after controlling for possible intersubject differences, was 0.0791 ($F(2, 368) = 15.8089$; $p < 0.001$). Normalized mean firing rate was significantly associated with motor index such that it was higher for neurons that reside closer to the motor output ($t = 5.3747$; $p < 0.001$). (D) Histogram showing the proportion of

variance explained between projections onto the SC slow drift axis and microsaccade rate. The median value across sessions is denoted by the dashed line. A p-value was computed by comparing the actual distribution of values to a null distribution (see Methods). $p < 0.05$*, $p < 0.01$**, $p < 0.001$***.

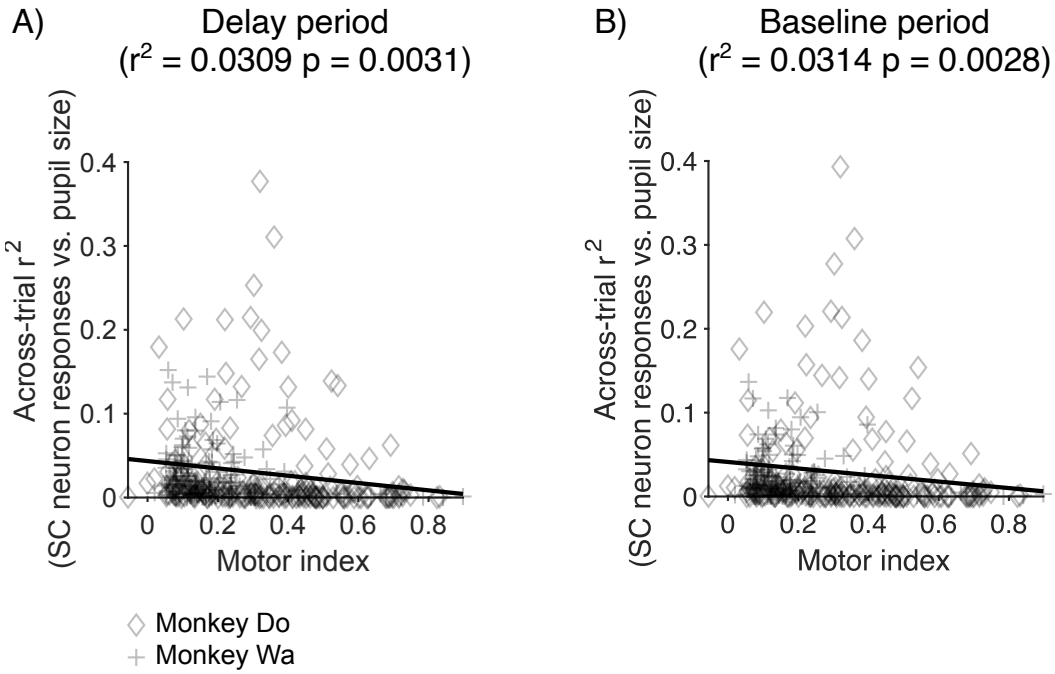

Figure 5 - figure supplement 1. Scatter plot showing the strength of the relationship between individual SC neuron responses and pupil size. In (A) pupil size was computed during the delay period whereas in (B) it was computed during the baseline period.